Engineering Science and Technology, an International Journal xxx (xxxx) xxx

HOSTED BY

ELSEVIER

Contents lists available at ScienceDirect

Engineering Science and Technology, an International Journal

journal homepage: www.elsevier.com/locate/jestch

Full Length Article

Computational modelling of multiphase fluid flow behaviour over a stretching sheet in the presence of nanoparticles

Sk. Reza-E-Rabbi [a], Sarder Firoz Ahmmed [b], S.M. Arifuzzaman [c], Tanmoy Sarkar [b], Md. Shakhaoath Khan [d,*]

[a] Department of Basic Sciences and Humanities, University of Asia Pacific, Dhaka 1207, Bangladesh
[b] Mathematics Discipline, Khulna University, Khulna 9208, Bangladesh
[c] Centre for Infrastructure Engineering, Western Sydney University, NSW 2751, Australia
[d] College of Science, Engineering and Health, RMIT University, VIC 3001, Australia

ARTICLE INFO

Article history:
Received 19 August 2018
Revised 24 June 2019
Accepted 20 July 2019
Available online xxxx

Keywords:
Casson and Maxwell fluids
Nanoparticles
Thermal radiation
Chemical reaction
Stretching sheet

ABSTRACT

Present study analysed hydrodynamic flow behaviour of multiphase radiative Casson and Maxwell fluids with the appearance of nano-sized particles. The impression of a nonlinear chemical reaction is also considered. Firstly, the time-dependent governing equations were computationally resolved using finite difference discretisation methods. Secondly, the convergence analysis with stabilisation of the numerical approach is carried out where the current model has converged for Le $\geq$ 0.025 and Pr $\geq$ 0.075. Finally, the impressions of various pertinent parameters are depicted diagrammatically along with tabular analysis on diversified flow fields. The main aim is to define and draw a comparison between Maxwell and Casson fluids on different flow fields. In addition, a comparative study between these two fluids is also newly carried out in this work through the analysis of streamlines and isotherms plotting. Furthermore, the thermal and mass properties found significantly improved mostly in the case of Maxwell fluid. However, Eckert number, Ec, has influenced the temperature field significantly for Casson fluid, and some parameters (Du, Nt, Nb, Le, Pr and Sr) have represented the identical impact on respective fields for both fluids. For the numerical validation, some comparisons are also shown with previous studies and satisfactory agreement is observed.

1. Introduction

In recent times, computational experiments in thermal radiative heat transfer through the hydromagnetic nanofluids flow have overwhelmed various scientists due to many industrial and manufacturing processes. Nanoparticles are used in engineering industries [1] due to its higher thermal conductivity properties compared to the base fluids. At the very beginning, the numerical investigations of a laminar flow due to stretching on a plane surface were inspected by Khan and Pop [2]. Bég et al. [3] experimented numerically, the characteristics of time-dependent hydromagnetic nanofluid flow, which was flowing over the exponential stretched surface. Their work was deliberated in a non-Darcian porous media. The algorithms of finite difference are still assigned widely because it yields stable and accurate outcomes. Explicit and implicit finite difference techniques are one of the fantastic consequences. By asserting these techniques, the following authors [4–10] depicted viscous dissipative time-dependent thermal radiative nanofluids flow numerically upon a stretching sheet. Diversified types of fluid were chosen for different aspects. Moreover, an explicit scheme was also implemented. A details stability test was also conducted for the accuracy of system parameters. Bachok et al. [11] inspected the properties of heat transfer for a nanofluid (H2O based) by considering three dissimilar nanoparticles viz. Cu, Al2O3 and TiO2. The flow was resulting from an exponentially shrinking/stretching surface and it revealed that for similarity solution the range of shrinking/stretching parameter was quite larger for exponential case rather than the usual linear and non-linear case. However, by implementing the method of a finite-element, the above-discussed nanoparticles were also inquired in a porous medium by Hussain [12]. On the other hand, in a flat tube, Zhao et al. [13] also did the analysis of the heat transfer properties with water basis nanofluid by taking only Al_2O_3 nanoparticle in a three-dimensional manner. By developing the impression of joule heating and viscous dissipation Hayat et al. [14] experimented the minimisation of entropy generation with Bejan number influence. Furthermore, Rashidi et al. [15] also carried out the analysis of entropy generation for a time-independent nanofluid flow in a porous rotating

* Corresponding author.
E-mail address: mohammad.shakhaoath.khan@rmit.edu.au (M.S. Khan).
Peer review under responsibility of Karabuk University.

https://doi.org/10.1016/j.jestch.2019.07.006
2215-0986/

Nomenclature

B	stretching/shrinking parameter, [–]
B_0	the magnetic component of the system, [Wbm^{-2}]
Cf	skin friction coefficient, [–]
C	non-dimensional concentration, [–]
c_p	specific heat of the system, [$Jkg^{-1}K^{-1}$]
C_w	concentration at the surface
C_∞	concentration away from the surface
C	concentration of nanoparticle
D_B	coefficient of Brownian diffusion
D_T	coefficient of thermophoresis diffusion
Du	Dufour number, [–]
Ec	Eckert number, [–]
Gr	thermal Grashof number, [–]
Gm	mass Grashof number, [–]
Kr	chemical reaction parameter, [–]
Le	Lewis number, [–]
M	magnetic parameter, [–]
Nb	Brownian parameter, [–]
Nt	thermophoresis parameter, [–]
Nu	heat transfer coefficient, [–]
Nv	Maxwell parameter, [–]
Pr	Prandtl number, [–]
Q	heat source, [–]
Ra	radiation parameter, [–]
Sh	Sherwood number, [–]
Sr	Soret number, [–]
T	fluid temperature, [K]
T_w	fluid temperature away at the surface
T_∞	fluid temperature away from the surface
$\bar{u}, \bar{v}$	velocity component in x, y-direction, [ms^{-1}]
u_w	stretching velocity, [ms^{-1}]
U, V	dimensionless velocity component, [–]

Greek symbols

τ	dimensionless time, [–]
λ_g	thermal conductivity, [$Wm^{-1}K^{-1}$]
λ_1	relaxation time effect, [s]
σ	Stefan-Boltzmann constant, [$Wm^{-2}K^{-4}$]

Abbreviations

EFDM	explicit finite difference method
MHD	magnetohydrodynamics
PDE	partial differential equation

disk. Besides, different sort of experiment for the analysis of entropy generation has also been done in diversified aspects. For explicit explanation, the reader can refer to the work of the following authors [16,17].

In fluid mechanics, the thermal and mass physiognomies of fluids flow such that non-Newtonian fluids flow resulting from a widening sheet has a vital role to play. It has a comprehensive range of applications in astrophysics, geophysics, modern technology etc. The shear stress and strain relations remain non-linear in the non-Newtonian fluid. Integral, differential and rate are three types of non-Newtonian fluid. Maxwell [18] introduced a non-Newtonian fluid, namely Maxwell fluid, which is a rate type fluid. The specialty of this fluid is, this model can count the relaxation time effects which cannot be described by other fluid models. The mass and thermal properties of a 2D Maxwell fluid flow have been speculated recently by some renowned researchers [19,20] with the appearance of thermophoresis and Joule heating. A numerical investigation was done by Shateyi [21] to discuss the behaviour of Maxwell fluid flowing over a vertical surface. Moreover, the impression of heat sink/source on Maxwell nanofluid and the attitude of stagnation point flow of the same fluid was displayed by these authors [22,23] in their corresponding work. Moreover, some reputed researchers have also done their research for time-dependent Maxwell fluid flow from different aspects and analysed the phenomena. For details, readers can refer to the following works [24–28].

Another kind of Non-Newtonian fluids that has recently attracted researchers is Casson fluid [29] (e.g., jelly, human blood, tomato sauce, honey, etc.) which depicts yield stress. Because of its shear thinning behaviour at the infinite shear rate, it exhibits zero viscosity and vice-versa. The potential applications of such fluids include processing of different nutrition, metallurgy, penetrating processes and bio-engineering manoeuvre. Newtonian heating and thermal radiation impression on a transient chemically reactive Casson fluid, which is flowing from a vertical flat plate were investigated by Das et al. [30]. By adopting the model of Casson nanofluid, Hayat et al. [31] explored mixed convective flow characteristics of this fluid over a stretched surface with heat sink/source and chemical reaction of linear order. Some reputed researchers also did their experiment with the very well-known Casson fluid. The purpose was to superintend the impression of homogeneous-heterogeneous reaction for the hydromagnetic Casson fluid flow on the stretched surface [32]. Raju and Sandeep [33] showed the non-linear radiative flow attitude of 3D Casson-Carreau fluids which is flowing from a stretching sheet while Mukhopadhyay et al. [34] conducted their experiment with Casson fluid only on the same discussed surface.

Recently, the numerical experiment of hydromagnetic Maxwell and Casson nanofluids flow due to stretching upon a plane surface were attempted by some researchers [35,36], where the incorporation of heat sink/source, chemical reaction, cross-diffusion was investigated. On the above-discussed investigations, the corresponding authors recapitulated the mass and heat transport attitude of some MHD flows by taking two or three physical influences. The inclusion of the magnetic field into the system carries more applied industrial applications in this research in particular: energy conversion, high-efficiency and low emission electric power generation, flow control vehicles, etc. Getting motivated by the work of above authors [35,36], the present analysis explored the impression of thermal radiation on 2D higher order MHD multiphase fluids flow due to stretching on a plane surface by envisaging different physical influences. The physical impacts of Casson parameter, Maxwell parameter, thermal radiation and viscous dissipation along with streamlines and isothermal analysis were unexplored by them, which is explored in this paper. The novel aspect of this work is to make a comparative study between Maxwell and Casson fluids and observe which fluid influence the thermal and mass properties more effectively. Also, to establish another relative phenomenon of those fluids through the analysis of streamlines and isotherms, this is done entirely new in this work.

2. Mathematical analysis

The behaviours of unsteady 2D chemically reactive Casson and Maxwell fluids flow with the existence of nanoparticles along with thermal radiation impression are apprehended in this article. Here, the order of a chemical reaction is non-linear. $\bar{u} = Bx$ is the fluid

Please cite this article as: S. Reza-E-Rabbi, S. F. Ahmmed, S. M. Arifuzzaman et al., Computational modelling of multiphase fluid flow behaviour over a stretching sheet in the presence of nanoparticles, Engineering Science and Technology, an International Journal, https://doi.org/10.1016/j.jestch.2019.07.006

velocity due to stretching and B is shrinking/stretching constant. B_0 is the magnetic field strength which is forced across at $y \geq 0$, this represents the direction of the fluid flow.

The fluid temperature, $\bar{T}$ and concentration, $\bar{C}$ get raised at t > 0, whereas near, and away from the wall, those are $\bar{T}_w$ & $\bar{C}_w$ and $\bar{T}_\infty$ & $\bar{C}_\infty$ respectively (Fig. 1). Considering the phenomena mentioned above, the principal equivalences within the boundary layers are taken as [9,21,24,25]:

$$\frac{\partial \bar{u}}{\partial x}+\frac{\partial \bar{v}}{\partial y}=0 \tag{1}$$

$$\begin{aligned}\frac{\partial \bar{u}}{\partial t}+\bar{u}\frac{\partial \bar{u}}{\partial x}+\bar{v}\frac{\partial \bar{u}}{\partial y}+\lambda_1\left(\bar{u}^2\frac{\partial^2 \bar{u}}{\partial x^2}+2\bar{u}\,\bar{v}\frac{\partial^2 \bar{u}}{\partial x\partial y}+\bar{v}^2\frac{\partial^2 \bar{u}}{\partial y^2}\right)\\ =\upsilon\left(1+\frac{1}{\beta}\right)\frac{\partial^2 \bar{u}}{\partial y^2}-\frac{\sigma B_0^2}{\rho}\bar{u}+g\beta_{\bar{T}}\left(\bar{T}-\bar{T}_\infty\right)+g\beta_{\bar{C}}\left(\bar{C}-\bar{C}_\infty\right)\\ -\left(1+\frac{1}{\beta}\right)\frac{\upsilon}{k_1}\bar{u}\end{aligned} \tag{2}$$

$$\begin{aligned}\frac{\partial \bar{T}}{\partial t}+\bar{u}\frac{\partial \bar{T}}{\partial x}+\bar{v}\frac{\partial \bar{T}}{\partial y}=\frac{\lambda_g}{\rho c_p}\frac{\partial^2 \bar{T}}{\partial y^2}+\left(1+\frac{1}{\beta}\right)\frac{\upsilon}{c_p}\left(\frac{\partial \bar{u}}{\partial y}\right)^2\\ +\tau\left[D_B\left(\frac{\partial \bar{C}}{\partial y}\frac{\partial \bar{T}}{\partial y}\right)+\frac{D_{\bar{T}}}{\bar{T}_\infty}\left(\frac{\partial \bar{T}}{\partial y}\right)^2\right]+\frac{D_m K_{\bar{T}}}{c_s c_p}\frac{\partial^2 \bar{C}}{\partial Y^2}\\ +\frac{\sigma B_0^2\bar{u}^2}{\rho c_p}+\frac{Q_0}{\rho c_p}\left(\bar{T}-\bar{T}_\infty\right)-\frac{1}{\rho c_p}\frac{\partial q_r}{\partial y}\end{aligned} \tag{3}$$

$$\frac{\partial \bar{C}}{\partial t}+\bar{u}\frac{\partial \bar{C}}{\partial x}+\bar{v}\frac{\partial \bar{C}}{\partial y}=D_B\frac{\partial^2 \bar{C}}{\partial y^2}-K_1\left(\bar{C}-\bar{C}_\infty\right)^p+\left(\frac{D_m K_{\bar{T}}}{\bar{T}_m}+\frac{D_{\bar{T}}}{\bar{T}_\infty}\right)\frac{\partial^2 \bar{T}}{\partial y^2} \tag{4}$$

With principal boundary conditions

$$\begin{aligned}&t=0,\ \bar{u}=Bx,\ \bar{v}=0,\bar{T}=\bar{T}_\infty,\ \bar{C}=\bar{C}_\infty && \text{everywhere}\\ &t\geqslant 0,\ \bar{u}=0,\ \bar{v}=0,\bar{T}=\bar{T}_\infty,\ \bar{C}=\bar{C}_\infty && \text{at } x=0\\ &\bar{u}=Bx,\ \bar{v}=0,\bar{T}=\bar{T}_w,\ \bar{C}=\bar{C}_w && \text{at } y=0\\ &\bar{u}=0,\ \bar{v}=0,\ \bar{T}\to\bar{T}_\infty,\ \bar{C}\to\bar{C}_\infty && \text{at } y\to\infty\end{aligned} \tag{5}$$

Here, the velocity components are $\bar{u}$ and $\bar{v}$ along x and y-axis. The relaxation time effect is λ_1, whereas λg denotes thermal conductivity. k_1 is the porous term, B (>0) and B (<0) are the stretching and shrinking constant, respectively, the kinematic viscosity is υ. At constant pressure, the specific heat is denoted by c_p. and the thermophoresis and Brownian diffusivity are D_T and D_B respectively.

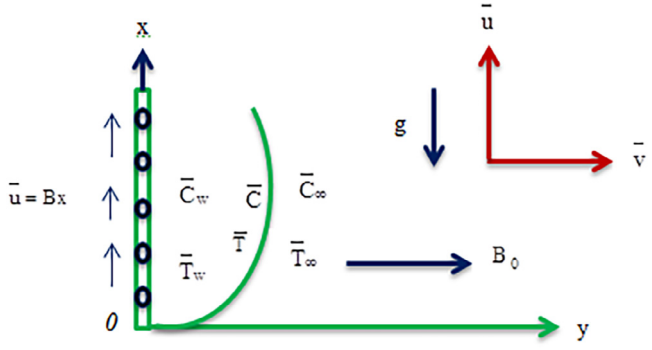

Fig. 1. Physical Illustration.

The thermal diffusion ratio and mass diffusivity are $D_{\bar{T}}$ and D_m, respectively. The expression can depict the approximation of Rosseland diffusion for radiative heat flux qr, $q_r=-(4\sigma'/3k_s)\left(\partial \bar{T}^4/\partial y\right)$, where, κ_s = mean absorption coefficient and σ' = Stefan-Boltzmann constant. It is considered that within the flow, the temperature variations are small enough and about $\bar{T}_\infty$ which express $\bar{T}^4$ in a Taylor series such that, $\bar{T}^4\approx 4\bar{T}_\infty^3\bar{T}-3\bar{T}_\infty^4$ (the higher terms are deducted). i.e., $\frac{\partial q_r}{\partial y}=-\frac{16\sigma'\bar{T}_\infty^3}{3k_s}\frac{\partial^2 \bar{T}}{\partial y^2}$.

Hence Eq. (3) becomes,

$$\begin{aligned}\frac{\partial \bar{T}}{\partial t}+\bar{u}\frac{\partial \bar{T}}{\partial x}+\bar{v}\frac{\partial \bar{T}}{\partial y}=\frac{\lambda_g}{\rho c_p}\frac{\partial^2 \bar{T}}{\partial y^2}+\left(1+\frac{1}{\beta}\right)\frac{\upsilon}{c_p}\left(\frac{\partial \bar{u}}{\partial y}\right)^2\\ +\tau\left[D_B\left(\frac{\partial \bar{C}}{\partial y}\frac{\partial \bar{T}}{\partial y}\right)+\frac{D_{\bar{T}}}{\bar{T}_\infty}\left(\frac{\partial \bar{T}}{\partial y}\right)^2\right]\\ +\frac{D_m K_{\bar{T}}}{c_s c_p}\frac{\partial^2 \bar{C}}{\partial Y^2}+\frac{\sigma B_0^2\bar{u}^2}{\rho c_p}+\frac{Q_0}{\rho c_p}\left(\bar{T}-\bar{T}_\infty\right)\\ +\frac{16\sigma'\bar{T}_\infty^3}{3k_s\rho c_p}\frac{\partial^2 \bar{T}}{\partial y^2}\end{aligned} \tag{6}$$

The non-dimensional variables are

$$U=\frac{\bar{u}}{U_0},V=\frac{\bar{v}}{U_0},Y=\frac{yU_0}{\upsilon},X=\frac{xU_0}{\upsilon},\tau=\frac{tU_0^2}{\upsilon},T=\frac{\bar{T}-\bar{T}_\infty}{\bar{T}_w-\bar{T}_\infty},$$
$$C=\frac{\bar{C}-\bar{C}_\infty}{\bar{C}_w-\bar{C}_\infty} \tag{7}$$

Therefore the dimensionless governing fluid flow model can be shifted in the underneath form:

$$\frac{\partial U}{\partial X}+\frac{\partial V}{\partial Y}=0 \tag{8}$$

$$\begin{aligned}\frac{\partial U}{\partial \tau}+U\frac{\partial U}{\partial X}+V\frac{\partial U}{\partial Y}=\left(1+\frac{1}{\beta}\right)\frac{\partial^2 U}{\partial Y^2}\\ -N\nu\left(U^2\frac{\partial^2 U}{\partial X^2}+2UV\frac{\partial^2 U}{\partial X\partial Y}+V^2\frac{\partial^2 U}{\partial Y^2}\right)\\ -MU+GrT+GmC-\left(1+\frac{1}{\beta}\right)KpU\end{aligned} \tag{9}$$

$$\begin{aligned}\frac{\partial T}{\partial \tau}+U\frac{\partial T}{\partial X}+V\frac{\partial T}{\partial Y}=\frac{1}{Pr}(1+Ra)\frac{\partial^2 T}{\partial Y^2}+\left(1+\frac{1}{\beta}\right)Ec\left(\frac{\partial U}{\partial Y}\right)^2\\ +Nb\left(\frac{\partial C}{\partial Y}\frac{\partial T}{\partial Y}\right)+Nt\left(\frac{\partial T}{\partial Y}\right)^2+Du\frac{\partial^2 C}{\partial Y^2}\\ +Ec\,MU^2+QT\end{aligned} \tag{10}$$

$$\frac{\partial C}{\partial \tau}+U\frac{\partial C}{\partial X}+V\frac{\partial C}{\partial Y}=\frac{1}{Le}\frac{\partial^2 C}{\partial Y^2}-Kr(C)^p+\left(\frac{Nt}{Nb\,Le}\right)\frac{\partial^2 T}{\partial Y^2}+Sr\frac{\partial^2 T}{\partial Y^2} \tag{11}$$

with boundary conditions,

$$\begin{aligned}&\tau\leqslant 0,\ U=0,\ V=0,T=0,\ C=0 && \text{everywhere}\\ &\tau>0,\ U=0,\ V=0,T=0,\ C=0 && \text{at } X=0\\ &U=BX=B,\ V=0,T=1,\ C=1 && \text{at } Y=0\\ &U=0,\ V=0,T=0,\ C=0 && \text{as } Y\to\infty\end{aligned} \tag{12}$$

Here, $N\nu=\lambda_1U_0^2/\upsilon$ is the Maxwell parameter, $M=\sigma B_0^2\upsilon/\rho U_0^2$ is the magnetic parameter, $Q=Q_0\upsilon/U_0^2\rho c_p$ is the heat source parameter, $Ra=16\sigma'\bar{T}_\infty^3/3k_s\lambda_g$ is the radiation parameter,

Please cite this article as: S. Reza-E-Rabbi, S. F. Ahmmed, S. M. Arifuzzaman et al., Computational modelling of multiphase fluid flow behaviour over a stretching sheet in the presence of nanoparticles, Engineering Science and Technology, an International Journal, https://doi.org/10.1016/j.jestch.2019.07.006

$Ec = U_0^2/c_p\left(\bar{T}_w - \bar{T}_\infty\right)$ is the Eckert number, $Pr = \upsilon\rho c_p/\lambda_g$ is the Prandtl number, $Le = \upsilon/D_B$ is the Lewis number, $Sr = \left(D_m K_{\bar{T}}/\bar{T}_m\upsilon\right)\left(\bar{T}_w - \bar{T}_\infty/\bar{C}_w - \bar{C}_\infty\right)$ is the Soret number, $Du = \left(D_m K_{\bar{T}}/c_s c_p \upsilon\right)\left[\left(\bar{C}_w - \bar{C}_\infty\right)/\left(\bar{T}_w - \bar{T}_\infty\right)\right]$ is the Dufour number, $Nb = \tau D_B\left(\bar{C}_w - \bar{C}_\infty\right)/\upsilon$ is the Brownian parameter, $Nt = \tau D_{\bar{T}}\left(\bar{T}_w - \bar{T}_\infty\right)/\bar{T}_\infty\upsilon$ is the thermophoresis parameter, $Kp = \upsilon^2/k_1 U_0^2$ is the Porous term, $Gr = \upsilon g\beta_{\bar{T}}\left(\bar{T}_w - \bar{T}_\infty\right)/U_0^3$ is the Grashof number, $Gm = \upsilon g\beta_{\bar{C}}\left(\bar{C}_w - \bar{C}_\infty\right)/U_0^3$ is the mass Grashof number, $Kr = \upsilon K_1\left(\bar{C}_w - \bar{C}_\infty\right)^{p-1}/U_0^2$ is the chemical reaction and p is the chemical reaction order.

For the existing problem, the local rate of mass transfer, heat transfer and local skin friction coefficients are depicted by the equations of the form as,

$$Sh = \frac{1}{\sqrt{2}}Gr^{-3/4}\left(\frac{\partial C}{\partial Y}\right)_{Y=0},\ Nu = \frac{1}{\sqrt{2}}Gr^{-3/4}\left(\frac{\partial T}{\partial Y}\right)_{Y=0} \text{ and}$$

$$Cf = -\frac{1}{2\sqrt{2}}\left(1+\frac{1}{\beta}\right)(1+\mathrm{Nv})Gr^{-3/4}\left(\frac{\partial U}{\partial Y}\right)_{Y=0}$$

3. Numerical computation

The dimensionless coupled PDEs are solved by exerting a known finite difference technique, namely explicit finite difference [37–41], within the given boundary conditions. Due to this fact, a flow field of rectangular shape is being considered, which is distributed by a grid of lines. These lines are collateral to X and Y axis (Fig. 2). In this paper, X_{max} (=100) and Y_{max} (=25) are the height of the plate as $Y \to \infty$. Furthermore, the numbers m = 125 and n = 125 are representing the grid space. What is more, $\Delta Y = 0.2(0 \leqslant Y \leqslant 25)$ and $\Delta X = 0.8(0 \leqslant X \leqslant 100)$ exhibit constant mesh sizes towards y and x-axis where the time step $\Delta\tau = 0.0005$ is sufficiently small.

Hence, Eqs. (8)–(12) become,

$$\frac{U_{i,j} - U_{i-1,j}}{\Delta X} + \frac{V_{i,j} - V_{i,j-1}}{\Delta Y} = 0 \tag{13}$$

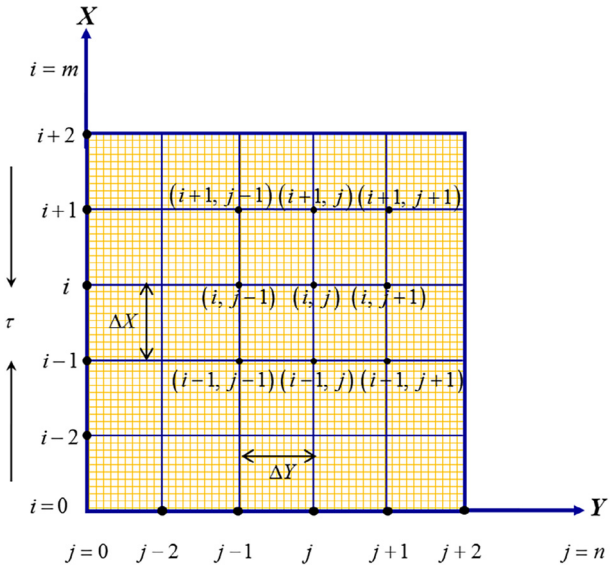

Fig. 2. Finite difference illustration.

$$\frac{U'_{i,j} - U_{i,j}}{\Delta\tau} + U_{i,j}\left(\frac{U_{i,j} - U_{i-1,j}}{\Delta X}\right) + V_{i,j}\left(\frac{U_{i,j+1} - U_{i,j}}{\Delta Y}\right) = \left(1+\frac{1}{\beta}\right)\left(\frac{U_{i,j+1} - 2U_{i,j} + U_{i,j-1}}{(\Delta Y)^2}\right)$$
$$- N\upsilon\left((U_{i,j})^2\frac{U_{i+1,j} - 2U_{i,j} + U_{i-1,j}}{(\Delta X)^2} + 2U_{i,j}V_{i,j}\frac{U_{i+1,j+1} - U_{i+1,j-1} - U_{i-1,j+1} + U_{i-1,j-1}}{4\Delta X\Delta Y} + (V_{i,j})^2\left(\frac{U_{i,j+1} - 2U_{i,j} + U_{i,j-1}}{(\Delta Y)^2}\right)\right)$$
$$- MU_{i,j} + Gr\,T_{i,j} + Gm\,C_{i,j} - \left(1+\frac{1}{\beta}\right)Kp\,U_{i,j} \tag{14}$$

$$\frac{T'_{i,j} - T_{i,j}}{\Delta\tau} + U_{i,j}\left(\frac{T_{i,j} - T_{i-1,j}}{\Delta X}\right) + V_{i,j}\left(\frac{T_{i,j+1} - T_{i,j}}{\Delta Y}\right) = \frac{1}{Pr}(1+Ra)$$
$$\times\left(\frac{T_{i,j+1} - 2T_{i,j} + T_{i,j-1}}{(\Delta Y)^2}\right) + \left(1+\frac{1}{\beta}\right)Ec\left(\frac{U_{i,j+1} - U_{i,j}}{\Delta Y}\right)^2$$
$$+ Nb\left(\frac{C_{i,j+1} - C_{i,j}}{\Delta Y}\right)\left(\frac{T_{i,j+1} - T_{i,j}}{\Delta Y}\right) + Nt\left(\frac{T_{i,j+1} - T_{i,j}}{\Delta Y}\right)^2$$
$$+ Du\left(\frac{C_{i,j+1} - 2C_{i,j} + C_{i,j-1}}{(\Delta Y)^2}\right) + Ec\,M(U_{i,j})^2 + QT_{i,j} \tag{15}$$

$$\frac{C'_{i,j} - C_{i,j}}{\Delta\tau} + U_{i,j}\left(\frac{C_{i,j} - C_{i-1,j}}{\Delta X}\right) + V_{i,j}\left(\frac{C_{i,j+1} - C_{i,j}}{\Delta Y}\right)$$
$$= \left(\frac{1}{Le}\right)\left(\frac{C_{i,j+1} - 2C_{i,j} + C_{i,j-1}}{(\Delta Y)^2}\right) - Kr(C_{i,j})^p$$
$$+ \left(Sr + \frac{Nt}{Nb\ Le}\right)\left(\frac{T_{i,j+1} - 2T_{i,j} + T_{i,j-1}}{(\Delta Y)^2}\right) \tag{16}$$

With boundary conditions,

$$U^n_{i,o} = 1,\ T^n_{i,o} = 1, C^n_{i,o} = 1$$
$$U^n_{i,o} = 0, T^n_{i,L} = 0, T^n_{i,L} = 0 \text{ where, } L \to \infty \tag{17}$$

Here, the meshing index are i and j lengthways X and Y axis, respectively.

4. Analysis of stability and convergence of the system

Due to the implementation of the explicit finite procedure, a stability test is required. For specific mesh sizes, it is possible to achieve the stability criterion for the remaining work in the following way, Eq. (13) does not contain $\Delta\tau$ because of that it will be deducted. $e^{i\alpha X}e^{i\beta Y}$ are typical relations of Fourier expansion for U, T and C at time $\tau = 0$ where, $i = \sqrt{-1}$. The following equations can be obtained at time τ and after a period respectively as,

Please cite this article as: S. Reza-E-Rabbi, S. F. Ahmmed, S. M. Arifuzzaman et al., Computational modelling of multiphase fluid flow behaviour over a stretching sheet in the presence of nanoparticles, Engineering Science and Technology, an International Journal, https://doi.org/10.1016/j.jestch.2019.07.006

$$\begin{array}{ll} U : D(\tau)e^{i\alpha X}e^{i\beta Y} & U : D'(\tau)e^{i\alpha X}e^{i\beta Y} \\ T : E(\tau)e^{i\alpha X}e^{i\beta Y} \quad \text{and} & T : E'(\tau)e^{i\alpha X}e^{i\beta Y} \\ C : F(\tau)e^{i\alpha X}e^{i\beta Y} & C : F'(\tau)e^{i\alpha X}e^{i\beta Y} \end{array} \tag{18}$$

Now applying Eq. (18) into Eqs. (14)–(16), by taking U, V as constants adoption,

$$\frac{(D'-D)e^{i\alpha X}e^{i\beta Y}}{\Delta\tau} + U\frac{De^{i\alpha X}e^{i\beta Y}\left(1-e^{-i\alpha\Delta X}\right)}{\Delta X} + V\frac{De^{i\alpha X}e^{i\beta Y}\left(e^{i\beta\Delta Y}-1\right)}{\Delta Y} = \left(1+\frac{1}{\beta}\right)2De^{i\alpha X}e^{i\beta Y}$$
$$\frac{(\cos\beta\Delta Y-1)}{(\Delta Y)^2} - Nv\left[\begin{array}{l} U^2\frac{2De^{i\alpha X}e^{i\beta Y}(1-\cos\alpha\Delta X)}{(\Delta X)^2} + V^2\frac{2De^{i\alpha X}e^{i\beta Y}(\cos\beta\Delta Y-1)}{(\Delta Y)^2} \\ +2UVDe^{i\alpha X}e^{i\beta Y}\frac{e^{i\alpha(X+\Delta X)}e^{i\beta(Y+\Delta Y)}-e^{i\alpha(X+\Delta X)}e^{i\beta(Y-\Delta Y)}}{4\Delta X\Delta Y} \\ -2UVDe^{i\alpha X}e^{i\beta Y}\frac{e^{i\alpha(X-\Delta X)}e^{i\beta(Y+\Delta Y)}-e^{i\alpha(X-\Delta X)}e^{i\beta(Y-\Delta Y)}}{4\Delta X\Delta Y} \end{array}\right]$$
$$-MDe^{i\alpha X}e^{i\beta Y} + Gr\,Ee^{i\alpha X}e^{i\beta Y} + Gm\,Fe^{i\alpha X}e^{i\beta Y} - \left(1+\frac{1}{\beta}\right)KpDe^{i\alpha X}e^{i\beta Y} \tag{19}$$

$$\frac{(E'-E)e^{i\alpha X}e^{i\beta Y}}{\Delta\tau} + U\frac{Ee^{i\alpha X}e^{i\beta Y}\left(1-e^{-i\alpha\Delta X}\right)}{\Delta X} + V\frac{Ee^{i\alpha X}e^{i\beta Y}\left(e^{i\beta\Delta Y}-1\right)}{\Delta Y} = \frac{1}{Pr}(1+Ra)2Ee^{i\alpha X}e^{i\beta Y}$$
$$\frac{(\cos\beta\Delta Y-1)}{(\Delta Y)^2} + \left(1+\frac{1}{\beta}\right)Ec\left(\frac{De^{i\alpha X}e^{i\beta Y}\left(e^{i\beta\Delta Y}-1\right)}{\Delta Y}\right)^2 + Nb\frac{Fe^{i\alpha X}e^{i\beta Y}\left(e^{i\beta\Delta Y}-1\right)}{\Delta Y}$$
$$\frac{Ee^{i\alpha X}e^{i\beta Y}\left(e^{i\beta\Delta Y}-1\right)}{\Delta Y} + Nt\left(\frac{Ee^{i\alpha X}e^{i\beta Y}\left(e^{i\beta\Delta Y}-1\right)}{\Delta Y}\right)^2 + Du\frac{2Fe^{i\alpha X}e^{i\beta Y}(\cos\beta\Delta Y-1)}{(\Delta Y)^2}$$
$$+Ec\,M\left(De^{i\alpha X}e^{i\beta Y}\right)^2 + Q\,Ee^{i\alpha X}e^{i\beta Y} \tag{20}$$

$$\frac{(F'-F)e^{i\alpha X}e^{i\beta Y}}{\Delta\tau} + U\frac{Fe^{i\alpha X}e^{i\beta Y}\left(1-e^{-i\alpha\Delta X}\right)}{\Delta X} + V\frac{Fe^{i\alpha X}e^{i\beta Y}\left(e^{i\beta\Delta Y}-1\right)}{\Delta Y} = \left(\frac{1}{Le}\right)$$
$$\frac{2Fe^{i\alpha X}e^{i\beta Y}(\cos\beta\Delta Y-1)}{(\Delta Y)^2} + \left(\frac{Nt}{Nb\,Le}+Sr\right)\left(\frac{2Ee^{i\alpha X}e^{i\beta Y}(\cos\beta\Delta Y-1)}{(\Delta Y)^2}\right) - Kr\left(Fe^{i\alpha X}e^{i\beta Y}\right)^p \tag{21}$$

Subsequently, Eqs. (19), (20) and (21) can be represented as,

$$\left.\begin{array}{l} D' = A_1D + A_2E + A_3F \\ E' = A_4E + A_5D + A_6F \\ F' = A_7F + A_8E \end{array}\right\} \tag{22}$$

where,

$$A_1 = 1 + \left(1+\frac{1}{\beta}\right)\frac{2\Delta\tau}{(\Delta Y)^2}(\cos\beta\Delta Y-1)$$
$$-Nv\left[U^2\frac{2\Delta\tau}{(\Delta X)^2}(1-\cos\alpha\Delta X) + V^2\frac{2\Delta\tau}{(\Delta Y)^2}(\cos\beta\Delta Y-1)\right.$$
$$+2UV\,\Delta\tau\frac{e^{i\alpha(X+\Delta X)}e^{i\beta(Y+\Delta Y)} - e^{i\alpha(X+\Delta X)}e^{i\beta(Y-\Delta Y)}}{4\Delta X\Delta Y}$$
$$\left.-2UV\Delta\tau\frac{e^{i\alpha(X-\Delta X)}e^{i\beta(Y+\Delta Y)} - e^{i\alpha(X-\Delta X)}e^{i\beta(Y-\Delta Y)}}{4\Delta X\Delta Y}\right] - M\Delta\tau$$
$$-\left(1+\frac{1}{\beta}\right)Kp\Delta\tau - U\frac{\Delta\tau}{\Delta X}\left(1-e^{-i\alpha\Delta X}\right) - V\frac{\Delta\tau}{\Delta Y}\left(e^{i\beta\Delta Y}-1\right)$$

$$A_2 = \Delta\tau\,Gr$$

$$A_3 = \Delta\tau\,Gm$$

$$A_4 = 1 + \tfrac{1}{Pr}(1+Ra)\tfrac{2\Delta\tau}{(\Delta Y)^2}(\cos\beta\Delta Y-1) + Nb\;C\tfrac{\Delta\tau}{(\Delta Y)^2}\left(e^{i\beta\Delta Y}-1\right)^2$$
$$+Nt\;T\tfrac{\Delta\tau}{(\Delta Y)^2}\left(e^{i\beta\Delta Y}-1\right)^2 + Q\Delta\tau - U\tfrac{\Delta\tau}{\Delta X}\left(1-e^{-i\alpha\Delta X}\right) - V\tfrac{\Delta\tau}{\Delta Y}\left(e^{i\beta\Delta Y}-1\right)$$

$$A_5 = A_5 = \left(1+\frac{1}{\beta}\right)Ec\,U\frac{\Delta\tau}{(\Delta Y)^2}\left(e^{i\beta\Delta Y}-1\right)^2 + Ec\;MU\Delta\tau$$

$$A_6 = Du\frac{2\Delta\tau}{(\Delta Y)^2}(\cos\beta\Delta Y-1)$$

$$A_7 = 1 + \left(\frac{1}{Le}\right)\frac{2\Delta\tau}{(\Delta Y)^2}(\cos\beta\Delta Y-1) - U\frac{\Delta\tau}{\Delta X}\left(1-e^{-i\alpha\Delta X}\right)$$
$$-V\frac{\Delta\tau}{\Delta Y}\left(e^{i\beta\Delta Y}-1\right) - \Delta\tau\,Kr(C)^{p-1}$$

$$A_8 = \left(\frac{Nt}{Nb\;Le}+Sr\right)\frac{2\Delta\tau}{(\Delta Y)^2}(\cos\beta\Delta Y-1)$$

The Eq. (22) can be elicited in the matrix shape as

$$\begin{bmatrix} D' \\ E' \\ F' \end{bmatrix} = \begin{bmatrix} A_1 & A_2 & A_3 \\ A_5 & A_4 & A_6 \\ 0 & A_8 & A_7 \end{bmatrix}\begin{bmatrix} D \\ E \\ F \end{bmatrix} \therefore \eta' = T'\eta \text{ where, } \eta' = \begin{bmatrix} D' \\ E' \\ F' \end{bmatrix},$$
$$T' = \begin{bmatrix} A_1 & A_2 & A_3 \\ A_5 & A_4 & A_6 \\ 0 & A_8 & A_7 \end{bmatrix} \text{ and } \eta = \begin{bmatrix} D \\ E \\ F \end{bmatrix}$$

For diversified values of $T'$the study is hard enough. Thus, a small time step is being taken i.e $\Delta\tau \to 0$. Accordingly, $A_2 \to 0, A_3 \to 0, A_5 \to 0, A_6 \to 0, A_8 \to 0$. Hence,

$$T' = \begin{bmatrix} A_1 & 0 & 0 \\ 0 & A_4 & o \\ 0 & 0 & A_7 \end{bmatrix}$$

$\lambda_1 = A_1$, $\lambda_2 = A_4$ and $\lambda_3 = A_7$ are the required Eigenvalues and these data must satisfy the following stability conditions, such that,

$$|A_1| \leqslant 1, |A_4| \leqslant 1, |A_7| \leqslant 1 \tag{23}$$

Considering,

$$a = \Delta\tau,\; b = U\frac{\Delta\tau}{\Delta X}, c = |-V|\frac{\Delta\tau}{\Delta X},\; d = 2\frac{\Delta\tau}{(\Delta Y)^2}, e = 2\frac{\Delta\tau}{(\Delta X)^2},$$
$$f = 2\frac{\Delta\tau}{\Delta X\Delta Y} \tag{24}$$

here, a, b, c, d, e and f all are real and non-negative numbers. Assuming, U and V are positive and negative, respectively. For $\alpha\Delta X = m\pi$ and $\beta\Delta Y = n\pi$,the highest modulus of A_1, A_4 and A_7 appear where, $n, m \neq$ even integers. Thus, using Eqs. (23) and (24) and considering the above conditions,

$$A_1 = 1 - 2\left[\left(1+\frac{1}{\beta}\right)d - \frac{Nv}{2}\left\{U^2e + V^2d + \frac{fUV}{4}\right\} + \frac{Ma}{2}\right.$$
$$\left.+\left(1+\frac{1}{\beta}\right)\frac{Kp\;a}{2} + b + c\right]$$

$$A_4 = 1 - 2\left[\frac{1}{Pr}(1+Ra)d - \frac{Qa}{2} - d\,Nt\,T - d\,Nb\;C + b + c\right]$$

$$A_7 = 1 - 2\left[\left(\frac{1}{Le}\right)d + \frac{a\,Kr(C)^{p-1}}{2} + b + c\right]$$

The utmost negative apprehended values of A_1, A_4 and A_7 are -1. Thus, the stability postulates are follows as,

$$\left(1+\frac{1}{\beta}\right)\frac{2\Delta\tau}{(\Delta Y)^2} - \frac{Nv}{2}\left[U^2\frac{2\Delta\tau}{(\Delta X)^2} + V^2\frac{2\Delta\tau}{(\Delta Y)^2} + \frac{UV}{4}\frac{2\Delta\tau}{\Delta X\Delta Y}\right] + \frac{M\Delta\tau}{2}$$
$$+\left(1+\frac{1}{\beta}\right)\frac{Kp\,\Delta\tau}{2} + U\frac{\Delta\tau}{\Delta X} + |-V|\frac{\Delta\tau}{\Delta Y} \leqslant 1$$

$$\tfrac{1}{Pr}(1+Ra)\tfrac{2\Delta\tau}{(\Delta Y)^2} - 2Nt\,T\tfrac{\Delta\tau}{(\Delta Y)^2} - 2Nb\,C\tfrac{\Delta\tau}{(\Delta Y)^2} - \tfrac{Q\Delta\tau}{2} + U\tfrac{\Delta\tau}{\Delta X} + |-V|\tfrac{\Delta\tau}{\Delta Y} \leqslant 1$$

and

$$\left(\frac{2}{Le}\right)\frac{\Delta\tau}{(\Delta Y)^2} + \frac{\Delta\tau\,Kr(C)^{p-1}}{2} + U\frac{\Delta\tau}{\Delta X} + |-V|\frac{\Delta\tau}{\Delta Y} \leqslant 1$$

Please cite this article as: S. Reza-E-Rabbi, S. F. Ahmmed, S. M. Arifuzzaman et al., Computational modelling of multiphase fluid flow behaviour over a stretching sheet in the presence of nanoparticles, Engineering Science and Technology, an International Journal, https://doi.org/10.1016/j.jestch.2019.07.006

here, $U = 0, V = 0, T = 0, C = 0$ at $\tau = 0$ are the primary boundary conditions. For, $\Delta\tau$ = 0.0005, ΔX = 0.8 and ΔY = 0.2, the convergence postulate for the existing work would be constituted as $Pr \geqslant 0.075$ *and* $Le \geqslant 0.025$.

5. Results and discussion

In this section, the elementary fluid properties due to the effects of physical constraints are conversed. Furthermore, the influences of some relevant parameters on Cf, Nu and Sh are analysed through a tabular presentation and graphically. However, these parameters behaviour on streamlines and isothermal lines are also discussed in details. Finally, some comparisons are being exhibited for the validation of this paper. The assumed values of the pertinent parameters are M = 4.0, 6.0, β = Nv = 0.2, Kr = 0.2, Ec = 0.01, Gr = 0.6, 10, Gm = 0.5, 5 Q = 1.0, p = Ra = 2.0, Sr = Du = 0.5, Kp = 1.0, B = 1.0, −1.0, Le = 1, Nt = 0.5, Nb = 0.3, 0.5 and Pr = 1.0, 7.0, 10.

Fig. 3 specifies the velocity fields for diversified values of M for stretching (B = 1.0) and shrinking (B = −1.0) case. It is obvious from the figure that in case of stretching, the boundary layers are going down in the field of velocity for boosting up the magnetic parameter.

Physically, higher M values yield a force, namely Lorentz force, which depreciates fluid flow. In the case of shrinking, Lorentz force enhances the streams in the velocity field as magnetic field intensity raises. Also, it is intriguing to observe that the Lorentz force is dominating Maxwell fluid flow significantly compared to Casson fluid flow. Fig. 4 shows the impression of porous media, Kp, on velocity outlines. It is found that velocity profiles are declining as the porous term rises from 0.5 to 2.0. The curve to curve decrement is 7.62% (0.5–1.0) and 9.32% (1.0–2.0) for Casson fluid whilst for Maxwell fluid the decrement is 2.31% (0.5–1.0) and 3.72% (1.0–2.0) at Y = 1.0086. Generally, porosity permits a major amount of fluids to be soaked from the boundary layer, for that reason, the flow field declines.

Fig. 5 demonstrated the fluid velocity vs. axis distribution, where the effect of Gr has been studied. It is observed that momentum boundary layers are developing as Grashof number increases because enhancement in thermal buoyancy force raises the velocity profiles. Herein the stream films of Maxwell fluid are more influenced by thermal buoyancy force than Casson fluid. The impression of radiation parameter, Ra, on time-dependent momentum boundary layers is displayed in Fig. 6. Here, the numerical data adopted for Casson and Maxwell fluid are 1.03296, 1.06959, 1.07884 and 2.03831, 2.08309, 2.09301 respectively for the diverse value of thermal radiation at Y = 1.0086. Physically, greater values of Ra help to reduce the mean captivation coefficient k_e and increase the

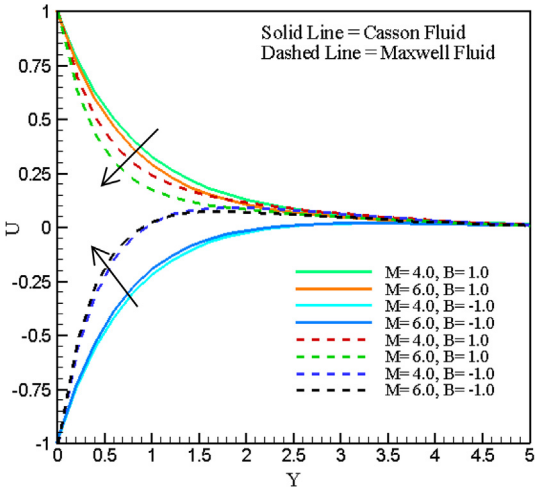

Fig. 3. Impact of M on U.

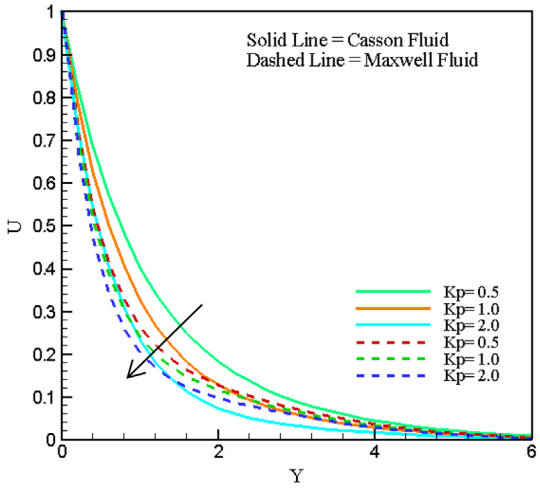

Fig. 4. Impact of Kp on U.

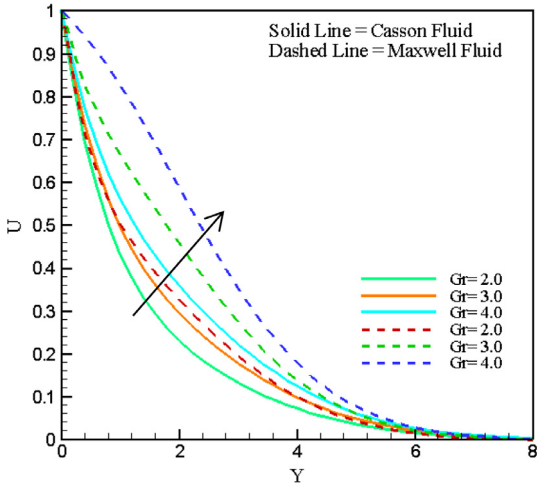

Fig. 5. Impact of Gr on U.

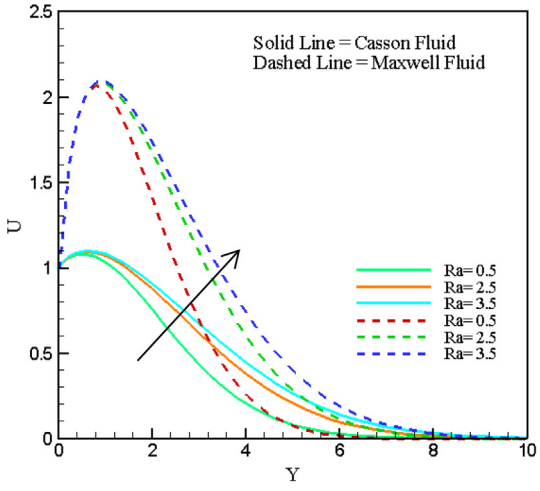

Fig. 6. Impact of Ra on U.

Please cite this article as: S. Reza-E-Rabbi, S. F. Ahmmed, S. M. Arifuzzaman et al., Computational modelling of multiphase fluid flow behaviour over a stretching sheet in the presence of nanoparticles, Engineering Science and Technology, an International Journal, https://doi.org/10.1016/j.jestch.2019.07.006

divergence of radiative flux. Also, from this observation, it can be concluded that velocity profiles are developing for rising radiation parameter, and the Maxwell fluid flows are influencing the velocity field significantly rather than Casson fluid flow.

Table 1 represents the dominance of Maxwell parameter, Nv, and Casson parameter, β, on velocity profiles. Both Maxwell and Casson parameters degenerate the velocity profiles. The table also exhibits the data fluctuation between the curve of Maxwell and Casson fluid flow.

For different Nt and Nb values, the temperature distribution is displayed in Figs. 7 and 8. Thermophoresis usually warms the flow streams and hence aggravates nanoparticle deprivation, which accentuates fluid velocity and finally develops the movement of nanoparticles. However, the identic impact is also seen for increasing Brownian parameter. The smaller size of nanoparticles corresponds with higher values of Nb, which assists in raising the distribution of fluid temperature. In this case, the boundary layers in temperature profiles are enhancing 5.97%, 6.75% and 5.88%, 6.65% respectively for Casson and Maxwell fluid with increasing (0.5–2.5) thermophoresis parameter. On the contrary, there is an enhancement of 3.18%, 2.74% and 3.21%, 2.76% in Casson and Maxwell fluid flow when the Brownian parameter varies (0.5–2.5).

On the other hand, Fig. 9 displays the influence of Nb on the nanoparticle concentric profiles. As it is mentioned earlier, larger values of Nb indicate the highest motion of the nanoparticle. Hence, for that reason, it is interesting to remark that the fluid mass distributions rise near the surface (Y = 0.40323) and reverse phenomena are observed away from the surface (Y = 1.20968). It is viewed from Fig. 10 that thermal boundary layers are boosting for increasing values (0.5–1.5) of Dufour number, Du. Usually, thermal and solutal buoyancy forces get an increase due to increment in Dufour number. Here, the fluctuations of curve increase 10.68% and 14.39% for Casson fluid whereas for Maxwell fluid the increment is 10.63% and 14.33% at Y = 1.0086. It is known that the fluid temperature gets enhance because increasing values of the dissipation parameter raise the buoyancy force.

Table 1
The numerical representation of Maxwell and Casson parameter on velocity profiles for stretching (B = 1.0) at Y = 1.00806.

β = Nv	U (for Nv)	U (for β)	Data fluctuation (%)
0.5	0.23947	0.29761	5.81%
1.5	0.23926	0.26719	2.79%
2.5	0.23914	0.25765	1.85%

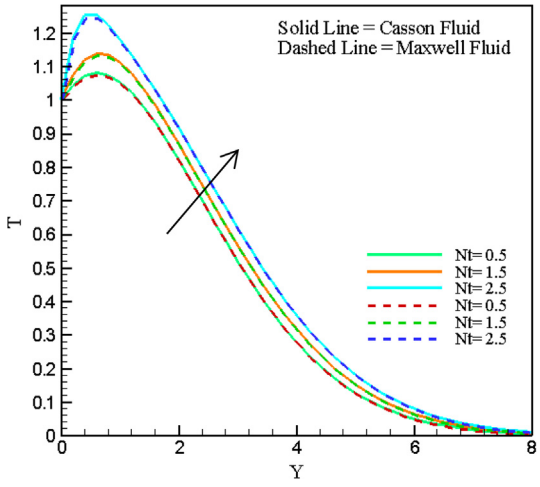

Fig. 7. Impact of Nt on T.

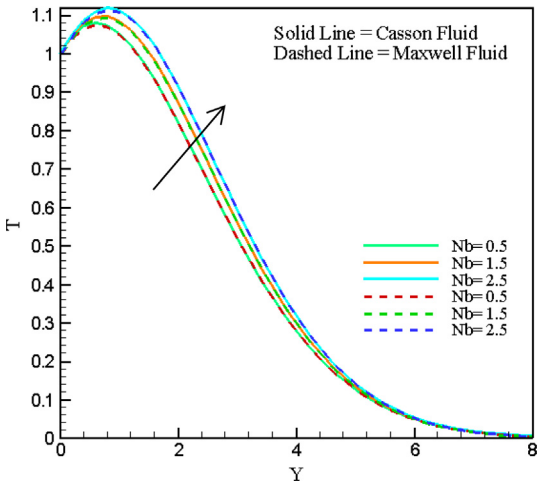

Fig. 8. Impact of Nb on T.

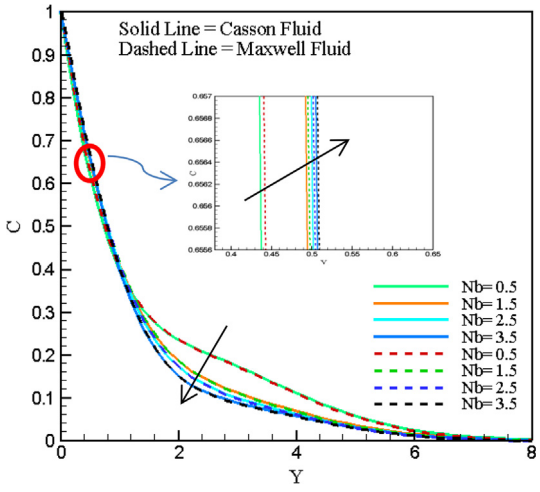

Fig. 9. Effects of Nb on C.

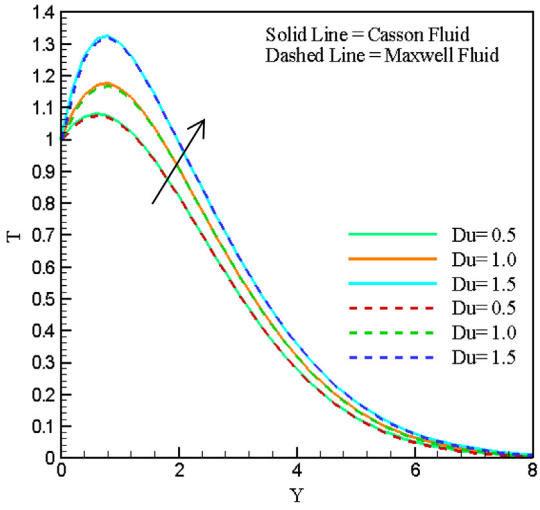

Fig. 10. Impact of Du on T.

This phenomenon is evident in Fig. 11. It is evident that the thermal flow layer is progressing as Eckert number, Ec increases from 0.01 to 0.07. From Fig. 12 displays disparity of fluid concentration

Please cite this article as: S. Reza-E-Rabbi, S. F. Ahmmed, S. M. Arifuzzaman et al., Computational modelling of multiphase fluid flow behaviour over a stretching sheet in the presence of nanoparticles, Engineering Science and Technology, an International Journal, https://doi.org/10.1016/j.jestch.2019.07.006

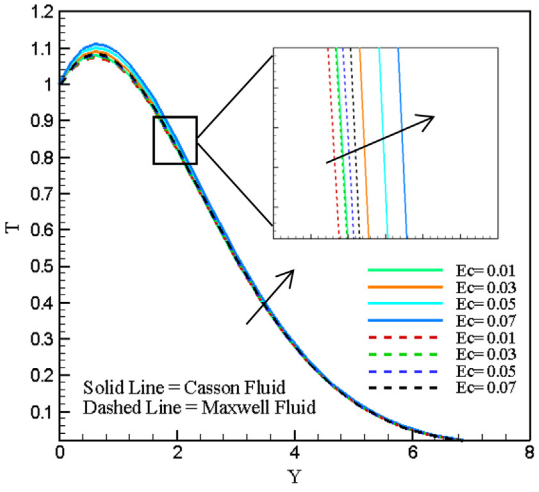

Fig. 11. Impact of Ec on T.

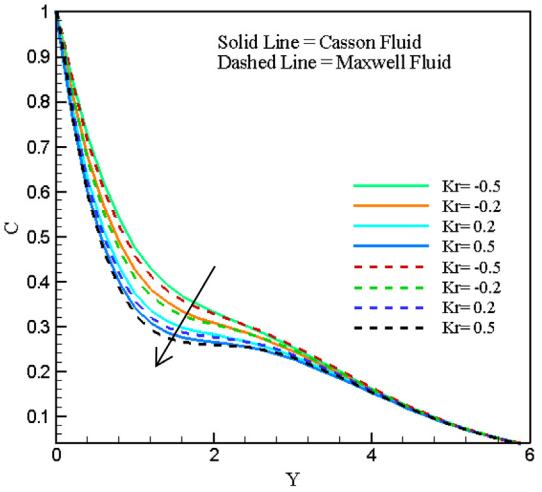

Fig. 13. Influence of Kr on C.

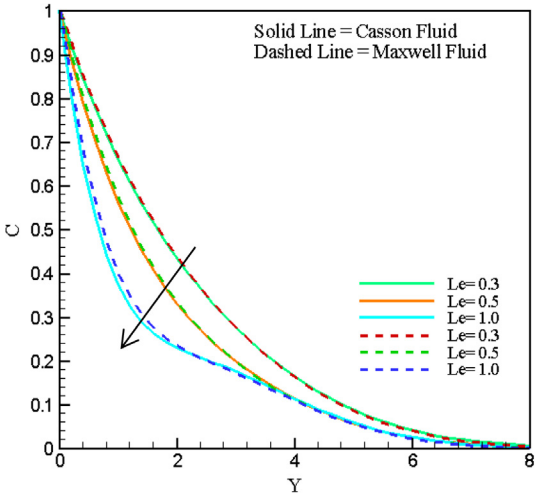

Fig. 12. Influence of Le on C.

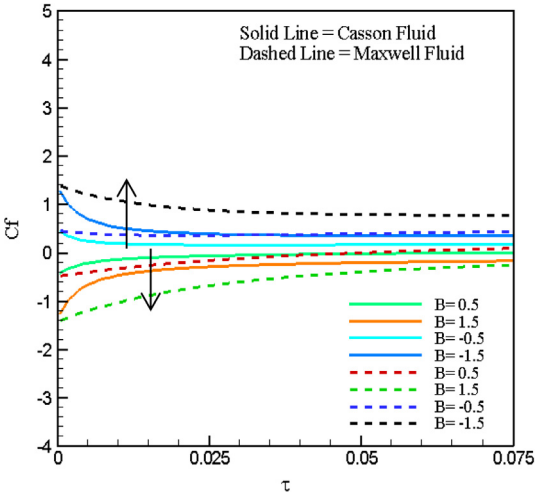

Fig. 14. Influence of B on Cf.

for varied Lewis number, Le, where, Le is the fraction of the thermal diffusivity to mass diffusivity and when the values of Le get to enhance the thermal diffusion rate goes beyond the rate of mass diffusion and eventually suppress the concentric field. This incident is observed in Fig. 12. The impact of destructive (Kr = 0.2, 0.5) and constructive (Kr = −0.5, −0.2) chemical reaction of order 2 on the nanoparticle concentric profiles are displayed in Fig. 13. It can be visualised that destructive chemical reaction parameters suppress the concentration profiles rapidly. Because it appears with several instabilities and implements high molecular motion, which elevates the transport phenomena and eventually decelerates the fluid concentration. The influence of stretching (B > 0) and shrinking (B < 0) parameters on skin friction profiles are depicted in Fig. 14. Herein due to the augmentation in stretching constraint, the skin friction outlines decrease. However, the opposite behaviour is seen for shrinking.

Moreover, Fig. 15 reflects that the increasing values of Sr diminish the Sherwood number profiles. Usually, Soret number generates additional mass flux which elevates fluid concentration, but at the wall, the rate of change of concentration is quite different. In the current numerical study, the dimensionless equations are solved with various transformations, because of that, the non-

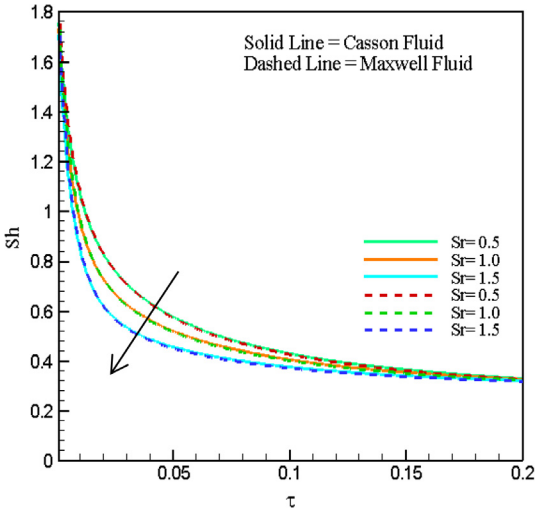

Fig. 15. Influence of Sr on Sh.

Please cite this article as: S. Reza-E-Rabbi, S. F. Ahmmed, S. M. Arifuzzaman et al., Computational modelling of multiphase fluid flow behaviour over a stretching sheet in the presence of nanoparticles, Engineering Science and Technology, an International Journal, https://doi.org/10.1016/j.jestch.2019.07.006

dimensional X and Y axis represents the entirely different mesh point. However, the boundary layer difference for various relevant parameters can be exhibited through isothermal and streamlines representation, which reflects the advanced visualisation of fluid flow.

Figs. 16–21 illustrate the analysis of streamlines and isothermal lines for both Maxwell fluid and Casson fluid. Fig. 16a displays that for Maxwell fluid, the velocity decreases as M rises, whereas the flood and line view of streamlines for Casson fluid with contour legend are also displayed in Fig. 16b. These phenomena arise because of Lorentz force, which is developed because of the influence of magnetic induction. In Fig. 17a, for Casson fluid, the thermal flow direction develops as thermal radiation constraint increases. Because the fluid molecules got heat up when the deviation of radiative heat flux increased. What is more, the flood and line view of an isothermal line for Maxwell fluid are also given with contour legend in Fig. 17b, which is represented with the same above discussed phenomena. Figs. 18a and 19b represent streamlines and isothermal analysis with the impact of Casson and Maxwell parameters. The flood and line view are also presented with contour

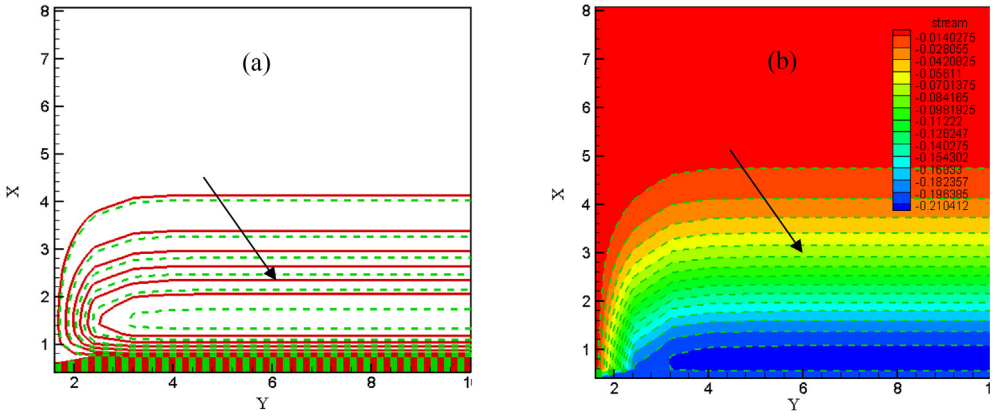

Fig. 16. (a) Streamlines (Maxwell fluid) for M = 0.5 (Red solid lines) and M = 1.5 (Green dashed lines). (b) Streamlines (Casson fluid) for M = 0.5, 1.5; (flood and line view).

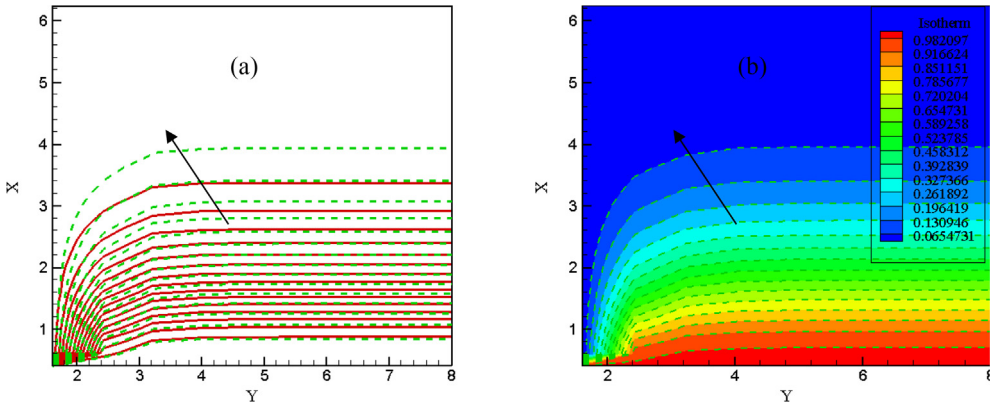

Fig. 17. (a) Isothermal lines (Casson fluid) for Ra = 0.5 (Red solid lines) and Ra = 1.5 (Green dashed lines), (b) Isothermal lines (Maxwell fluid) for Ra = 0.5, 1.5; (flood and line view).

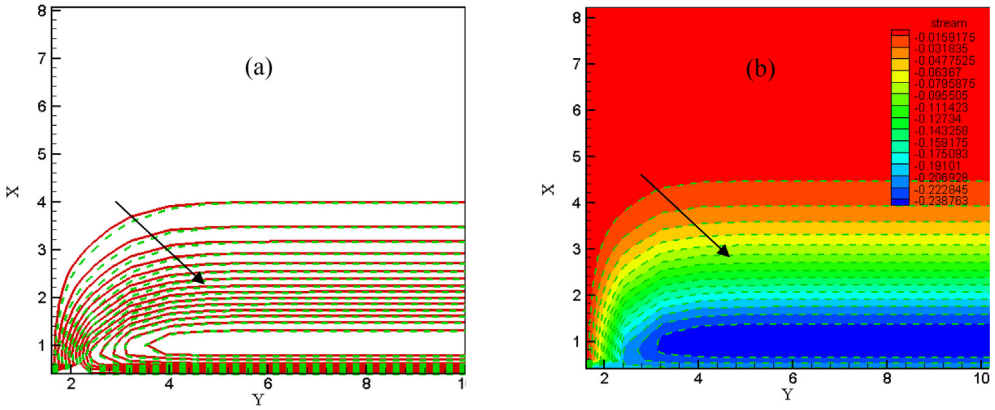

Fig. 18. (a) Streamlines (Maxwell fluid) for Nv = 0.2 (Red solid lines) and Nv = 0.4 (Green dashed lines), (b) Streamlines (Casson fluid) for β = 0.2, 0.4; (flood and line view).

Please cite this article as: S. Reza-E-Rabbi, S. F. Ahmmed, S. M. Arifuzzaman et al., Computational modelling of multiphase fluid flow behaviour over a stretching sheet in the presence of nanoparticles, Engineering Science and Technology, an International Journal, https://doi.org/10.1016/j.jestch.2019.07.006

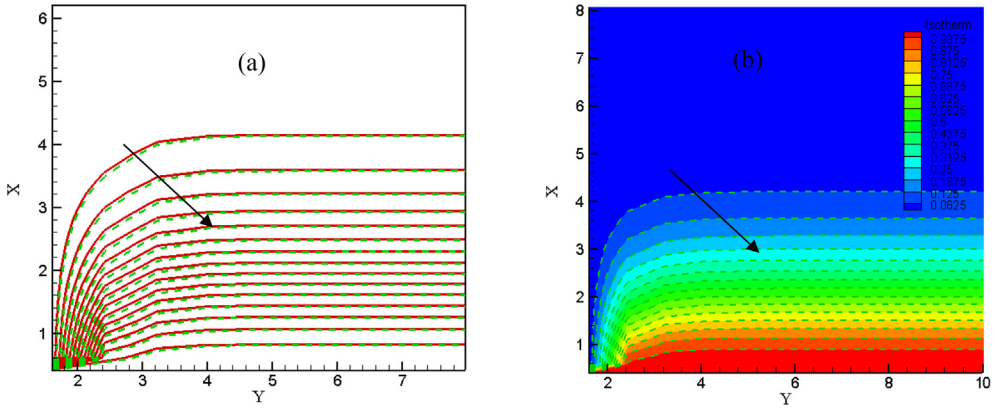

Fig. 19. (a) Isothermal lines (Casson fluid) for β = 0.2 (Red solid lines) and β = 0.4 (Green dashed lines), (b) Isothermal lines (Maxwell fluid) for Nv = 0.2, 0.4; (flood and line view).

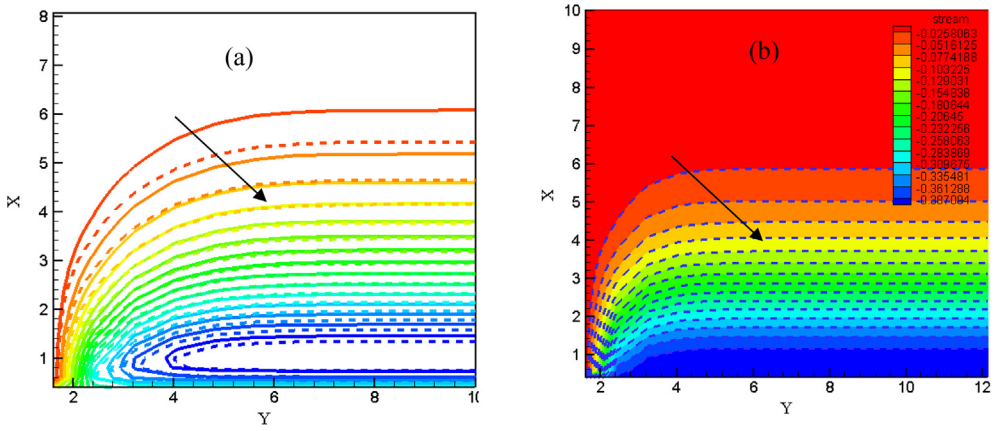

Fig. 20. (a) Streamlines (Maxwell fluid) for Pr = 7.0 (solid lines) and Pr = 10 (dashed lines), (b) Streamlines (Casson fluid) for Pr = 7.0, 10.0; (flood and line view).

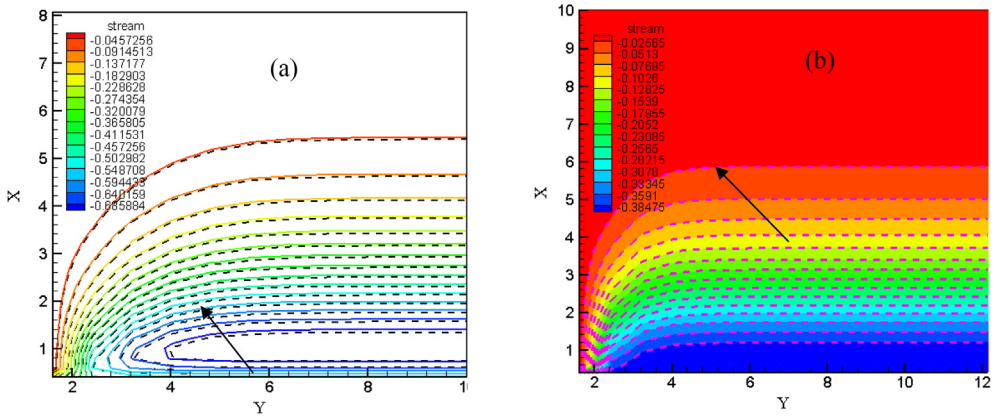

Fig. 21. (a) Streamlines (Maxwell fluid) for Kr = 0.5, when p (order) = 1, 2; (dashed lines (order 1)) and (solid lines (order 2)), (b) Streamlines (Casson fluid) for Kr = 0.5, when p (order) = 1, 2; (flood and line view).

levels. In these figures, the momentum and thermal boundary layers both are diminishing as Casson and Maxwell parameter increases. The conduction and convection rates usually vary for different fluids. Additionally, it is known that the Prandtl number, Pr, is used unevenly to control where the convection or conduction process will dominate. Generally, for Pr > 1 momentum diffusivity influences. This phenomenon is evident in Fig. 20a and b for both Maxwell and Casson fluids. As the value of Pr gets to increase the thickness of the momentum boundary layers declines. Because Pr is contrariwise proportionate to thermal diffusivity therefore fluid heat reduced for developing Pr and eventually the thermal as well as momentum boundary layers getting reduced. The impact of linear and non-linear order chemical reaction has been analysed theoretically through the analysis of streamlines in Fig. 21a and b. It is depicted that when the order of the chemical reaction is being increased the momentum boundary layers got an increase for both

Please cite this article as: S. Reza-E-Rabbi, S. F. Ahmmed, S. M. Arifuzzaman et al., Computational modelling of multiphase fluid flow behaviour over a stretching sheet in the presence of nanoparticles, Engineering Science and Technology, an International Journal, https://doi.org/10.1016/j.jestch.2019.07.006

fluids and interestingly it is found that the impact of chemical reaction order was more influential for Maxwell fluid. Physically, the above phenomena took place in the existence of higher order destructive chemical reaction appears with much more disturbances rather than the linear one. Due to this disturbance, the transport phenomena develops and finally helps in raising the viscosity of momentum boundary layers. Moreover, through the analysis of streamlines and isothermal lines, it has been inspected that the heat and mass properties are influencing the flow fields significantly for the cases of Maxwell fluid.

Tables 2 and 3 exhibit the encouragement of some physical constraints on Cf, Nu and Sh for Casson and Maxwell fluid. It can be seen that Dufour number, heat radiation and generation parameters enhance friction factor and mass transfer coefficient profiles while these parameters suppress the Nusselt number profiles for both fluids. Also, the magnetic and porous parameters degenerate the skin friction profiles, whereas chemical reaction doesn't show any indicatory change on friction factor. Furthermore, Kr develops the mass transfer coefficient profiles while M and Kp do not give any variations on it, and Kr also represents no visible change in

Table 2
Physical parameters (Cf, Nu and Sh) of Casson fluid.

M	Du	Kr	Kp	R	Q	Cf	Nu	Sh
2.0	0.5	0.2	1	2	1	−0.40609	1.04269	1.26520
4.0						−0.40836	1.04267	1.26520
6.0						−0.41062	1.04266	1.26520
	0.5					−0.40609	1.04269	1.26520
	1.0					−0.40519	0.95409	1.28684
	1.5					−0.40429	0.87318	1.30879
		0.1				−0.40609	1.04269	1.26517
		0.2				−0.40609	1.04269	1.26520
		0.3				−0.40609	1.04269	1.26523
			0.5			−0.40265	1.04268	1.26520
			1.0			−0.40609	1.04269	1.26520
			1.5			−0.40949	1.04270	1.26520
				1.0		−0.40941	1.21233	1.22292
				2.0		−0.40609	1.04269	1.26520
				3.0		−0.40117	0.91442	1.29951
					1.0	−0.40609	1.04269	1.26520
					2.0	−0.40607	1.04059	1.26549
					3.0	−0.40606	1.03848	1.26579

Table 3
Physical parameters (Cf, Nu and Sh) of Maxwell fluid.

M	Du	Kr	Kp	R	Q	Cf	Nu	Sh
2.0	0.5	0.2	1	2	1	−0.76061	1.05072	1.17383
4.0						−0.76150	1.05072	1.17383
6.0						−0.76239	1.05072	1.17383
	0.5					−0.76150	1.05072	1.17383
	1.0					−0.76024	0.96762	1.20085
	1.5					−0.75896	0.88162	1.22840
		0.1				−0.76150	1.05072	1.17378
		0.2				−0.76150	1.05072	1.17383
		0.3				−0.76150	1.05072	1.17387
			0.5			−0.76128	1.05072	1.17383
			1.0			−0.76150	1.05072	1.17383
			1.5			−0.76173	1.05072	1.17383
				1.0		−0.76370	1.22173	1.11816
				2.0		−0.76150	1.05072	1.17383
				3.0		−0.75891	0.92131	1.21901
					1.0	−0.76061	1.05072	1.17383
					2.0	−0.76108	1.04863	1.17421
					3.0	−0.76107	1.04653	1.17459

Table 4
Comparison of the outcomes with published papers.

Increased Parameter	Present Result			Kumar et al. [35]			Kumaran and Sandeep [36]		
	U	T	C	U	T	C	U	T	C
M	Decr			Decr			Decr		
Nt		Incr			Incr				
Nb		Incr	Decr		Incr	Decr			Decr
Le			Decr		Incr	Decr		Incr	Decr
Kr			Decr			Decr		Incr	
Du		Incr						Incr	

Incr = Increase, Decr = Decrease.

Please cite this article as: S. Reza-E-Rabbi, S. F. Ahmmed, S. M. Arifuzzaman et al., Computational modelling of multiphase fluid flow behaviour over a stretching sheet in the presence of nanoparticles, Engineering Science and Technology, an International Journal, https://doi.org/10.1016/j.jestch.2019.07.006

Table 5
The effects of Le on Sh (effect comparison through numerical data).

This study			Kumar et al. [35]			Kumaran and Sandeep [36]		
Le	Sh		Le	Sh		Le	Sh	
	Casson	Maxwell		Casson	Maxwell		Casson	Maxwell
0.3	0.97685	0.97957	0.5	0.082447	0.065954	0.5	0.447966	0.456161
0.6	1.19195	1.19885	0.6	0.164045	0.147250	1.0	0.729884	0.738350
0.9	1.25145	1.25527	0.7	0.238678	0.221811	1.5	0.978069	0.986097

Table 6
Comparison table for Nu when Nv = M = Kp = Ec = Du = Q = Sr = Kr = p = 0, Casson term is absent and Pr = Le = 10.

Parameter Nt = Nb	Nu (This study)	Nu (Khan et al. [5])
0.1	0.9574	0.9541
0.2	0.3605	0.3667
0.3	0.1329	0.1359
0.4	0.0491	0.0499
0.5	0.0193	0.0179

Nusselt number for both fluids. Also, magnetic parameter reduces, and porous term raises heat transfer rates for Casson fluid, while, interestingly they don't exert any indicatory changes for Maxwell fluid. From Table 4, it is evident that the qualitative impressions of the following parameters are the same as the published literature such that they are in good agreement. Also, Table 5 explains the impact of Le on mass transfer coefficient profiles.

Here the effect of Le has been compared through numerical data. In all three works, rising values of Le help to develop the Sherwood number profiles for both Casson and Maxwell fluids. Moreover, in Table 6, the numerical data for various Nt, Nb on Nu have compared, and they are in good agreement. Hence Tables 4–6 establish the validation of the existing work.

6. Conclusions

The theoretical examination is conducted to exhibit the impression of radiation on 2D hydromagnetic chemically reactive Casson and Maxwell nanofluids, which is flowing over a stretched surface. The outcome of this study can be briefly listed below:

a. Due to increment in Grashof number, radiation and magnetic parameters (for shrinking), the boundary layers are progressing in the fields of velocity. On the contrary, the up-surging values of magnetic (for stretching), Casson, Maxwell and Porous parameters depreciate the flow fields.
b. Progressing values of Eckert number, Dufour number, Brownian and thermophoresis parameters are helping to boost the thickness of thermal boundary layers.
c. Increasing values of Brownian, Lewis number and chemical reaction have a propensity to decline the boundary layers in the concentration fields while it is quite impressive to see that for rising values of Brownian parameter the concentric profiles are developing initially close to the wall.
d. When the values of shrinking (B < 1), Dufour number, radiation and heat source parameters are raising, then the profiles of Cf (skin friction) are going up whereas up surging values of magnetic, porous and stretching (B > 1) parameters are diminishing the Cf profiles. However, chemical reaction shows no indicatory change in Cf.
e. The heat transfer coefficient profiles are rising due to increment in porous parameter, Kp (Casson fluid) but for Maxwell fluid, Kp does not show any same changes in Nu (Nusselt number). While the increasing data of magnetic, radiation and heat source parameters along with Dufour number are helping to go down the Nu profiles. Also, for Maxwell fluid magnetic parameter represents no change in Nu.
f. The profiles of Sh (Sherwood number) are improving when the data of Dufour number, chemical reaction, radiation and heat source parameters increase. On the other hand, Sh profiles are falling due to enhancement in Soret number. Moreover, magnetic and porous parameters do not display any significant change in Sh for both fluids.
g. The streamlines are falling when the data of magnetic, Prandtl number, Casson and Maxwell parameters get to raise, and the contrary event observed for developing values of p (order of chemical reaction). What is more, increasing values of radiation are building up the isothermal lines, whereas progressing data of Casson and Maxwell parameters tend to depreciate the isothermal lines.

References

[1] J. Buongiorno, Convective transport in nanofluids, J. Heat Transfer 128 (2005) 240–250.
[2] W.A. Khan, I. Pop, Boundary-layer flow of a nanofluid past a stretching sheet, Int. J. Heat Mass Transf. 53 (2010) 2477–2483.
[3] O.A. Bég, M.S. Khan, I. Karim, M.M. Alam, M. Ferdows, Explicit numerical study of unsteady hydromagnetic mixed convective nanofluid flow from an exponentially stretching sheet in porous media, Appl. Nanosci. 4 (2014) 943–957.
[4] M.S. Khan, M.M. Alam, M. Ferdows, Effects of magnetic field on radiative flow of a nanofluid past a stretching sheet, Procedia Eng. 56 (2013) 316–322.
[5] M.S. Khan, I. Karim, L.E. Ali, A. Islam, Unsteady MHD free convection boundary-layer flow of a nanofluid along a stretching sheet with thermal radiation and viscous dissipation effects, Int. Nano Lett. 2 (2012) 24.
[6] Sk. Reza-E-Rabbi, S.M. Arifuzzaman, T. Sarkar, M.S. Khan, S.F. Ahmmed, Explicit finite difference analysis of an unsteady MHD flow of a chemically reacting Casson fluid past a stretching sheet with Brownian motion and thermophoresis effects, J. King Saud Univ. Sci. (2018). in press.
[7] S.M. Arifuzzaman, M.S. Khan, A. Al-Mamun, Sk. Reza-E-Rabbi, P. Biswas, I. Karim, Hydrodynamic stability and heat and mass transfer flow analysis of MHD radiative fourth-grade fluid through porous plate with chemical reaction, J. King Saud Univ. Sci. (2019). in press.
[8] S.M. Arifuzzaman, M.S. Khan, M.F.U. Mehedi, B.M.J. Rana, S.F. Ahmmed, Chemically reactive and naturally convective high-speed MHD fluid flow through an oscillatory vertical porous-plate with heat and radiation absorption effect, Eng. Sci. Technol. Int. J. 21 (2) (2018) 215–228.
[9] S.M. Arifuzzaman, M.S. Khan, M.S. Islam, M.M. Islam, B.M.J. Rana, P. Biswas, S.F. Ahmmed, MHD Maxwell fluid flow in presence of nano-particle through a vertical porous–plate with heat-generation, radiation absorption and chemical reaction, Front. Heat Mass Transfer 9 (2017) 1–14.
[10] A.A. Mamun, S.M. Arifuzzaman, Sk. Reza-E-Rabbi, P. Biswas, M.S. Khan, Computational modelling on MHD radiative Sisko nanofluids flow through a nonlinearly stretching sheet, Int. J. Heat Technol. 37 (1) (2019) 285–295.
[11] N. Bachok, A. Ishak, I. Pop, Boundary layer stagnation-point flow and heat transfer over an exponentially stretching/shrinking sheet in a nanofluid, Int. J. Heat Mass Transf. 55 (25–26) (2012) 8122–8128.
[12] S. Hussain, Finite element solution for MHD flow of nanofluids with heat and mass transfer through a porous media with thermal radiation, viscous dissipation and chemical reaction effects, Adv. Appl. Math. Mech. 9 (4) (2017) 904–923.
[13] N. Zhao, J. Yang, H. Li, Z. Zhang, S. Li, Numerical investigations of laminar heat transfer and flow performance of Al2O3–water nanofluids in a flat tube, Int. J. Heat Mass Transf. 92 (2016) 268–282.
[14] T. Hayat, S. Qayyum, M.I. Khan, A. Alsaedi, Entropy generation in magnetohydrodynamic radiative flow due to rotating disk in presence of viscous dissipation and Joule heating, Phys. Fluids 30 (2018) 017101.

Please cite this article as: S. Reza-E-Rabbi, S. F. Ahmmed, S. M. Arifuzzaman et al., Computational modelling of multiphase fluid flow behaviour over a stretching sheet in the presence of nanoparticles, Engineering Science and Technology, an International Journal, https://doi.org/10.1016/j.jestch.2019.07.006

[15] M.M. Rashidi, S. Abelman, N. Freidooni Mehr, Entropy generation in steady MHD flow due to a rotating porous disk in a nanofluid, Int. J. Heat Mass Transf. 62 (2013) 515–525.
[16] S. Hussain, K. Mehmood, M. Sagheer, MHD mixed convection and entropy generation of water–alumina nanofluid flow in a double lid driven cavity with discrete heating, J. Magn. Magn. Mater. 419 (2016) 140–155.
[17] M.W. Ahmed Khan, M.I. Khan, T. Hayat, A. Alsaedi, Entropy generation minimization (EGM) of nanofluid flow by a thin moving needle with nonlinear thermal radiation, Physica B 534 (2018) 113–119.
[18] J.C. Maxwell, On the dynamical theory of gases, Philos. Trans. R. Soc. Lond. 157 (1867) 49–88.
[19] T. Hayat, M. Qasim, Influence of thermal radiation and Joule heating on MHD flow of a Maxwell fluid in the presence of thermophoresis, Int. J. Heat Mass Transf. 53 (2010) 4780–4788.
[20] T. Hayat, R. Sajjad, Z. Abbas, M. Sajid, A.A. Hendi, Radiation effects on MHD flow of Maxwell fluid in a channel with porous medium, Int. J. Heat Mass Transf. 54 (2011) 854–862.
[21] S. Shateyi, A new numerical approach to MHD flow of a Maxwell fluid past a vertical stretching sheet in the presence of thermophoresis and chemical reaction, Boundary Value Problems 196 (2013).
[22] G.K. Ramesh, B.J. Gireesha, Influence of heat source/sink on a Maxwell fluid over a stretching surface with convective boundary condition in the presence of nanoparticles, Ain Shams Eng. J. 5 (2014) 991–998.
[23] G.K. Ramesh, B.J. Gireesha, T. Hayat, A. Alsaedi, Stagnation point flow of Maxwell fluid towards a permeable surface in the presence of nano particles, Alexandria Eng. J. 55 (2016) 857–865.
[24] M. Madhu, N. Kishan, A.J. Chamkha, Unsteady flow of a Maxwell nanofluid over a stretching surface in the presence of magnetohydrodynamic and thermal radiation effects, Propul. Power Res. 6 (2017) 31–40.
[25] S. Palani, B.R. Kumar, P.K. Kameswaran, Unsteady MHD flow of an UCM fluid over a stretching surface with higher order chemical reaction, Ain Shams Eng. J. 7 (2016) 399–408.
[26] S. Mukhopadhyay, Heat transfer analysis of the unsteady flow of a Maxwell fluid over a stretching surface in the presence of a heat source/sink, Chin. Phys. Lett. 29 (2012) 054703.
[27] S.K. Nandy, Unsteady flow of Maxwell fluid in the presence of nanoparticles toward a permeable shrinking surface with Navier slip, J. Taiwan Inst. Chem. Eng. 000 (2015) 1–9.
[28] M. Shen, S. Chen, F. Liu, Unsteady MHD fow and heat transfer of fractional Maxwell viscoelastic nanofuid with Cattaneo heat flux and different particle shapes, Chinese J. Phys. (2018). in press.
[29] N. Casson, A flow equation for pigment oil suspensions of the printing ink type, in: C.C. Mill (Ed.), Rheology of Disperse Systems, Advances in Mechanical Engineering, Pergamon Press, Oxford, 1959.
[30] M. Das, R. Mahato, R. Nandkeolyar, Newtonian heating effect on unsteady hydromagnetic Casson fluid flow past a flat plate with heat and mass transfer, Alexandria Eng. J. 54 (2015) 871–879.
[31] T. Hayat, A.M. Bilal, S.A. Shehzad, A. Alsaedi, Mixed convection flow of Casson nanofluid over a stretching sheet with convectively heated chemical reaction and heat source/sink, J. Appl. Fluid Mech. 8 (2015) 803–811.
[32] M.I. Khan, M. Waqas, T. Hayat, A. Alsaedi, A comparitive study of Casson fluid with homogeneous-heterogeneous reactions, J. Colloid Interface Sci. 498 (2017) 85–90.
[33] C.S.K. Raju, N. Sandeep, Unsteady three-dimensional flow of Casson-Carreau fluids past a stretching surface, Alexandria Eng. J. 55 (2016) 1115–1126.
[34] S. Mukhopadhyay, P.R. De, K. Bhattacharyya, G.C. Layek, Casson fluid flow over an unsteady stretching surface, Ain Shams Eng. J. 4 (2013) 933–938.
[35] M.S. Kumar, N. Sandeep, B.R. Kumar, S. Saleem, A comparative study of chemically reacting 2D flow of Casson and Maxwell fluids, Alexandria Eng. J. (2017) 1110–10168.
[36] G. Kumaran, N. Sandeep, Computational analysis of magnetohydrodynamic Casson and Maxwell flows over a stretching sheet with cross diffusion, Results Phys. 7 (2016) 147–155.
[37] S.M. Arifuzzaman, P. Biswas, M.F.U. Mehedi, S.F. Abdullah Al-Mamun, M.S. Khan Ahmmed, Analysis of unsteady boundary layer viscoelastic nanofluid flow through a vertical porous plate with thermal radiation and periodic magnetic field, J. Nanofluids 7 (2018) 1122–1129.
[38] S.M. Arifuzzaman, M.F.U. Mehedi, P. Abdullah Al-Mamun, R. Biswas, M.S. Khan Islam, Magnetohydrodynamic micropolar fluid flow in presence of nanoparticles through porous plate: a numerical study, Int. J. Heat Technol. 36 (2018) 936–948.
[39] P. Biswas, S.M. Arifuzzaman, M.M. Rahman, M.S. Khan, Effects of periodic magnetic field on 2D transient optically dense gray nanofluid over a vertical plate: a computational EFDM study with SCA, J. Nanofluids 7 (2018) 82–91.
[40] P. Biswas, S.M. Arifuzzaman, I. Karim, M.S. Khan, Impacts of magnetic field and radiation absorption on mixed convective jeffrey nano fluid flow over a vertical stretching sheet with stability and convergence analysis, J. Nanofluids 6 (2017) 1082–1095.
[41] S.M. Arifuzzaman, M.S. Khan, K.E. Hossain, M.S. Islam, S. Akter, R. Roy, Chemically reactive viscoelastic fluid flow in presence of nano particle through porous stretching sheet, Front. Heat Mass Transfer 9 (2017) 1–12.

Please cite this article as: S. Reza-E-Rabbi, S. F. Ahmmed, S. M. Arifuzzaman et al., Computational modelling of multiphase fluid flow behaviour over a stretching sheet in the presence of nanoparticles, Engineering Science and Technology, an International Journal, https://doi.org/10.1016/j.jestch.2019.07.006